

## THE FRACTURE MECHANICS FORMULAS FOR SPLIT-TENSION STRIPS

RAGIP INCE

*Firat University, Engineering Faculty, Civil Engineering Department, Elazig, Turkey*

*e-mail: rince@firat.edu.tr*

The notched beams have been commonly used in concrete fracture. In this study, the splitting-strip specimens, which have some advantages – compactness and lightness – compared to beams, are analyzed for effective crack models. Using the Fourier integrals and Fourier series, a formula for the maximum tensile strength of concrete is first derived for an un-notched splitting-strip in the plane of loading. Subsequently, the linear elastic fracture mechanics formulas of the splitting-strip specimens, namely the stress intensity factor  $K_I$ , the crack mouth opening displacement  $CMOD$ , and the crack opening displacement profile  $COD$ , are determined for different load-distributed widths via the weight function.

*Keywords:* concrete, Fourier integrals, fracture mechanics, splitting test, weight functions

### 1. Introduction

The split-tension specimens are frequently used to determine tensile strength of materials, such as concrete and rock (Neville, 2011). The split-cylinder test, which is also called the Brazilian split test, was proposed by Carneiro and Barcellos (1949). This test was successfully applied to cubes by Nilsson (1961). However, split-tension test specimens, namely, cylinders, cubes and diagonal cubes, have also been successfully used in concrete fractures over the last decade (Modeer, 1979; Tang, 1994; Rocco *et al.*, 1995; Tang *et al.*, 1996; Ince, 2010, 2012a,b). The splitting concrete specimens exhibit several advantages, e.g., compactness and lightness, and the weight of the specimen can be disregarded in calculation of fracture parameters.

The experimental investigations on fracture mechanics of cement-based materials conducted until the 1970s indicated that classical linear elastic fracture mechanics (LEFM) was no longer valid for quasi-brittle materials such as concrete. This inapplicability of LEFM was due to the existence of a relatively large inelastic zone in the front and around the tip of the main cracks in concrete. This so-called fracture process zone (FPZ) was ignored by LEFM. Consequently, several investigators have developed deterministic fracture-mechanics approaches to describe fracture-dominated failure of concrete structures. These models could be classified as cohesive crack models and effective crack models. Contrary to LEFM, in which a single fracture parameter was used such as the critical stress intensity factor, those models needed at least two experimentally determined fracture parameters to characterize failure of concrete structures. These models could be classified as cohesive crack models and effective crack models: namely the two-parameter model (Jenq and Shah, 1985), the effective crack model (Nallathambi and Karihaloo, 1986), the size effect model (Bazant and Kazemi, 1990) and the double-K model (Xu and Reinhardt, 1999).

Analytical and numerical studies on split-tension specimens (Modeer, 1979; Tang, 1994; Rocco *et al.*, 1995; Tang *et al.*, 1996; Ince, 2010, 2012a,b; Ince *et al.*, 2015, 2016) have revealed that nominal strength is highly affected by the width of the distributed load and the specimen size. The existing design codes have not considered these effects in the determination of the split-tensile strength of concrete. On the other hand, theoretical and experimental studies with

splitting strip specimens (Davies and Bose, 1968; Filon, 1903; Schlee, 1978) are limited when compared to those of other splitting specimens.

For this purpose, LEFM formulas for the stress intensity factor  $K_I$ , the crack mouth opening displacement ( $CMOD$ ), and the crack opening displacement profile ( $COD$ ) of splitting strip specimens have been evaluated for different load-distributed widths and initial crack lengths utilizing the weight function in this study. In addition, the maximum tensile stresses in the un-notched split-tension strips have also been determined for different load-distributed widths.

## 2. A historical overview of splitting tests

As indicated in Fig. 1a, a split-tension specimen is placed between the platens of the test machine and the load is subsequently applied until failure, which is caused by splitting along the vertical diameter due to the lateral tensile stress that has occurred (Neville, 2011). According to elasticity theory (Timoshenko and Godier, 1970), the nominal tensile strength of split-tension specimens is defined as

$$\sigma_{Nc} = \frac{2P_c}{\pi b h} \quad (2.1)$$

where  $P_c$  is the ultimate load,  $b$  is the specimen width and  $h$  is the specimen depth. However, Eq. (2.1) is only valid for the concentrated loading condition shown in Fig. 1a. In practice, the applied load is distributed on the specimens over a finite width ( $2t$ ) using soft materials, such as hard cardboard and plywood, as indicated in Fig. 1b (Neville, 2011; Davies and Bose, 1960). Tang *et al.* (1992) investigated the effect of distributed load in three-point bending beams and split-tension cylinders. The nominal strength decreased with the increasing width of the distributed load in the split-tension cylinder, whereas this effect was not significant in the bending specimens. According to Tang (1994), the maximum tensile stress value of the un-notched cylinder specimens at the plane of loading could be calculated as

$$\sigma_{max} = \frac{2P}{\pi b h} \sqrt{(1 - \beta^2)^3} \quad (2.2)$$

where  $P$  is the total compressive load and  $\beta = 2t/h = t/d$  is the ratio of the distributed-load width to the specimen depth ( $d$  is the characteristic specimen size), as depicted in Fig. 1. Rocco *et al.* (1995) examined the cylinder and cube specimens and proposed that the maximum tensile stress could be calculated for the un-notched cube specimens at the plane of loading as follows

$$\sigma_{max} = \frac{2P}{\pi b h} \left[ \sqrt[3]{(1 - \beta^2)^5} - 0.0115 \right] \quad \beta \leq 0.20 \quad (2.3)$$

Using the boundary element method, a formula for the maximum tensile strength of concrete was similarly derived for un-notched diagonal cubes in the plane of loading by Ince (2012a) as follows

$$\sigma_{max} = \frac{2P}{\pi b h} \frac{1}{0.931 + 38.931\beta^{4.778}} \quad \beta \leq 0.25 \quad (2.4)$$

One of the advantages of diagonal splitting-cube specimens is nearly  $\text{const} = 1/0.931 = 1.074$  maximum stress in the plane of loading for  $\beta \leq 0.15$ , which differs from other splitting specimens.

Approaches based on fracture mechanics and using notched split cylinder specimens were first performed by Tweed *et al.* (1972). They developed a closed-form expression for the geometry factor of the notched split-tension cylinder. Tang (1994) also used the finite element method

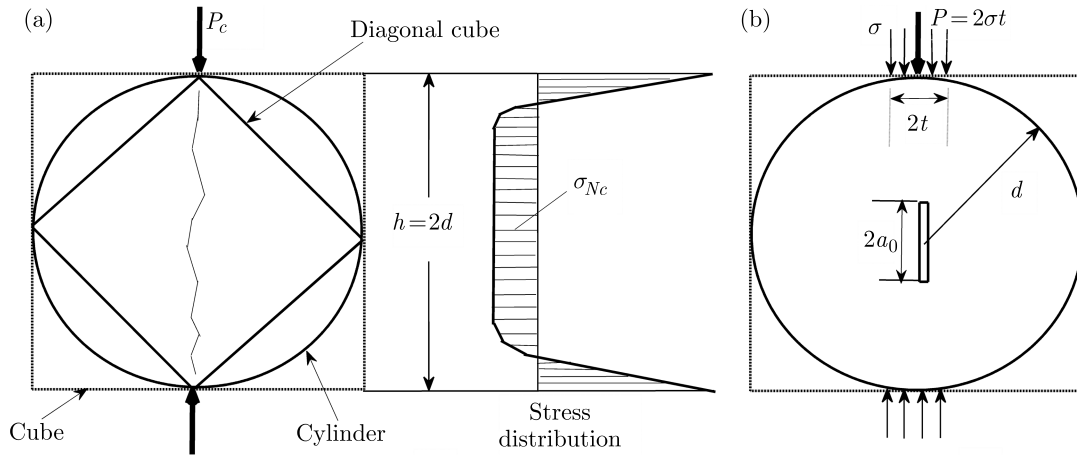


Fig. 1. Splitting tension test: (a) geometry and stress distribution, (b) notched specimen and distributed loading case

to study notched cylinder specimens under the opposite distributed loading and the developed LFM formulas (Fig. 1b). Cubical and diagonal cubic specimens with a central notch were investigated using effective crack models by Ince (2010, 2012a) who evaluated LFM formulas with those split-tension specimens for various load-distributed widths and initial crack lengths using the finite element and boundary element method. A series of experimental studies with split-tension and beam specimens were also performed. The results were discussed based on two most popular fracture models: the two-parameter and the size effect models. The results of the tests revealed that the notched cube and diagonal cube tests can be utilized successfully for determining the fracture parameters of concrete. Subsequently, Ince (2012b) derived an improved version of LFM formulas for splitting cylinder and cube specimens and then computed the four-term universal weight functions of the split-tension specimens such as cylinder, cube and diagonal cube by using the boundary element method to simulate the double-K concrete fracture model.

The numbers of theoretical and experimental studies with splitting strip specimens (Davies and Bose, 1968; Filon, 1903; Schlee, 1978) were limited when compared to studies conducted with other splitting specimens. For instance, a formula similar to equations (2.2)-(2.4) was not developed. Therefore, in the present research, both un-notched and notched splitting strip specimens have been analyzed using analytical and numerical methods.

### 3. Deriving LFM formulas for split-tension strip

In this study, split-tension strip specimens have been simulated for the use in effective crack fracture models based on earlier studies of split-tension tests for concrete fracture. The weight function approach was used to determine the LFM formulas for split-tension strip specimens with the central initial notch.

The weight function method was originally suggested by Bueckner (1970) and Rice (1972) to evaluate the stress intensity factor using a simple integration. When a weight function is determined for a notched body, the stress intensity factors could be calculated for arbitrary loadings on the same body. For the case of mode I, the stress intensity factors can be expressed as follows

$$K_I = \int_0^a \sigma(y)m(y, a) dy \quad (3.1)$$

where  $a$  is the crack length,  $\sigma(y)$  is the normal stress along the crack line in the un-cracked body, and  $m(y, a)$  is the weight function (or Green's functions which are essentially equivalent to the weight functions) (Gdoutos, 1990).

For the central notch, an infinite strip subjected to four equal point loads on the notch, as shown in Fig. 2, the Green function was derived by Tada *et al.* (2000) as follows

$$K_I = \frac{2F}{\sqrt{2d}} \left[ +0.297 \sqrt{1 - \left(\frac{y}{a}\right)^2} \left(1 - \cos \frac{\pi a}{2d}\right) \right] \sqrt{\tan \frac{\pi a}{2d}} \left[ 1 - \left(\cos \frac{\pi a}{2d} / \cos \frac{\pi y}{2d}\right)^2 \right]^{-\frac{1}{2}} \quad (3.2)$$

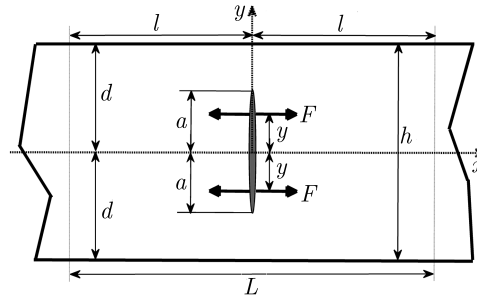


Fig. 2. A center-cracked infinite strip subjected to four equal point loads

The accuracy of Eq. (3.2) is better than 1% for all  $a/d$  and  $y/a$  (Tada *et al.*, 2000). The normal stresses along the crack line in the un-cracked body must be first computed to determine the stress intensity factor according to the weight function method.

### 3.1. Determination of normal stresses along the crack line in the un-cracked body

In this study, a rectangular plate  $-l < x < l$  and  $-d < y < d$  with unit width is only loaded by a uniform compressive traction  $p_0$  in the central region  $-t < x < t$  of both boundaries  $y = \pm d$ . It is modeled by considering earlier studies on split-tension tests (Ince, 2010, 2012a,b), as depicted in Fig. 3a. In the plane elasticity problems not including body forces, the stress components can be expressed via the following equations (Barber, 2004; Timoshenko and Godier, 1970)

$$\sigma_x = \frac{\partial^2 \Phi}{\partial y^2} \quad \sigma_y = \frac{\partial^2 \Phi}{\partial x^2} \quad \tau_{xy} = -\frac{\partial^2 \Phi}{\partial x \partial y} \quad (3.3)$$

in which  $\Phi$  is the so-called Airy's stress function of  $x$  and  $y$ . This function also satisfies the following bi-harmonic equation

$$\frac{\partial^4 \Phi}{\partial x^4} + 2 \frac{\partial^4 \Phi}{\partial x^2 \partial y^2} + \frac{\partial^4 \Phi}{\partial y^4} = 0 \quad (3.4)$$

A stress function based on a polynomial can be utilized for some simple cases such as a continuously distributed loading on the boundaries of the elastic body. However, a more useful solution for discontinuous loading, as shown in Fig. 3a, may be derived by using Fourier series (Barber, 2004; Timoshenko and Godier, 1970; Mirsalimov and Hasanov, 2015; Basu and Mandal, 2016). The following equation has commonly been used as the stress function in such cases

$$\Phi = \sin(\lambda x) f(y) \quad \lambda = \frac{n\pi}{l} \quad (3.5)$$

where  $n$  is an integer and  $f(y)$  is only a function of  $y$ . When Eq. (3.5) is substituted into Eq. (3.4) in order to determine  $f(y)$ , the following ordinary differential equation is obtained

$$f^{(4)}(y) - 2\lambda^2 f''(y) + \lambda^4 f(y) = 0 \quad (3.6)$$

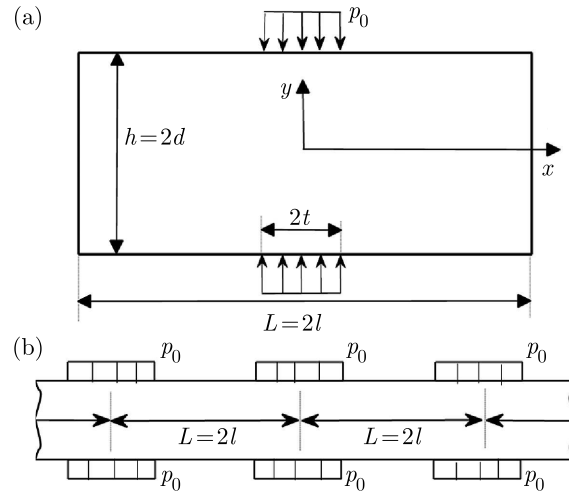


Fig. 3. (a) Base problem for split-tension strip, (b) case of periodic loading

The general solution to the above equation can be written as

$$f(y) = C_1 \cosh(\lambda y) + C_2 \sinh(\lambda y) + C_3 y \cosh(\lambda y) + C_4 y \sinh(\lambda y) \tag{3.7}$$

Consequently, the stress function of the given problem is

$$\Phi = \sin(\lambda x)[C_1 \cosh(\lambda y) + C_2 \sinh(\lambda y) + C_3 y \cosh(\lambda y) + C_4 y \sinh(\lambda y)] \tag{3.8}$$

in which  $C_1, C_2, C_3$  and  $C_4$  are arbitrary constants. Since the loading and geometry of the plate in Fig. 3a are symmetric in both axes, and  $\sinh(\lambda y)$  and  $y \cosh(\lambda y)$  are odd functions, the constants  $C_2$  and  $C_3$  are equal to zero (Barber, 2004). Therefore, the stress components can be determined from Eq. (3.3) as follows

$$\begin{aligned} \sigma_x &= \sin(\lambda x)\{C_1 \lambda^2 \cosh(\lambda y) + C_4 \lambda[2 \cosh(\lambda y) + \lambda y \sinh(\lambda y)]\} \\ \sigma_y &= -\lambda^2 \sin(\lambda x)\{C_1 \cosh(\lambda y) + C_4 y \sinh(\lambda y)\} \\ \tau_{xy} &= -\lambda \cos(\lambda x)\{C_1 \lambda \sinh(\lambda y) + C_4[\sinh(\lambda y) + \lambda y \cosh(\lambda y)]\} \end{aligned} \tag{3.9}$$

When the loading given in Fig. 3a is expanded into the Fourier series, the following equation can be obtained

$$p(x) = \frac{p_0 t}{l} + \frac{2p_0}{l} \sum_{n=1}^{\infty} \frac{1}{\lambda} \sin(\lambda t) \cos(\lambda x) \tag{3.10}$$

where the first term gives the mean load. The constants  $C_1$  and  $C_4$  in Eqs. (3.8) and (3.9) can be determined from the following boundary conditions

$$\begin{aligned} y = \pm d &\Rightarrow \tau_{xy} = 0 \\ y = \pm d &\Rightarrow \sigma_y = p(x) \end{aligned} \tag{3.11}$$

Substituting the first boundary condition in Eq. (3.9)<sub>3</sub>, the following equation can be written as

$$C_4 = -C_1 \frac{\lambda \sinh(\lambda d)}{\sinh(\lambda d) + \lambda d \cosh(\lambda d)} \tag{3.12}$$

A similar procedure with Eq. (3.9)<sub>2</sub> and the second boundary conditions can be carried out for the corresponding constants as

$$\begin{aligned} C_1 &= \frac{p(x)}{\lambda^2 \sin(\lambda x)} \frac{\sinh(\lambda d) + \lambda d \cosh(\lambda d)}{\cosh(\lambda d) \sinh(\lambda d) + \lambda d} \\ C_4 &= -\frac{p(x)}{\lambda^2 \sin(\lambda x)} \frac{\lambda \sinh(\lambda d)}{\cosh(\lambda d) \sinh(\lambda d) + \lambda d} \end{aligned} \tag{3.13}$$

Consequently, the normal stress  $\sigma_x$  can be derived from Eq. (3.9)<sub>1</sub> as

$$\sigma_x = \frac{2p_0}{\pi} \sum_{n=1}^{\infty} \frac{\psi_n(\lambda, y)}{n} \sin(\lambda t) \cos(\lambda x) \quad (3.14)$$

$$\psi_n(\lambda, y) = \frac{\cosh(\lambda y)[\lambda d \cosh(\lambda d) - \sinh(\lambda d)] - \lambda y \sinh(\lambda d) \sinh(\lambda y)}{\cosh(\lambda d) \sinh(\lambda d) + \lambda d}$$

For the case of the concentrated load, the above equation can be converted into the following form since  $2p_0 t = P = \text{const}$  and  $\lim_{\lambda \rightarrow 0} \sin(\lambda)/\lambda = 1$  in which  $\lambda = n\pi/l$

$$\sigma_x = \frac{P}{l} \sum_{n=1}^{\infty} \psi_n(\lambda, y) \cos(\lambda x) \quad (3.15)$$

Nevertheless, Equations (3.14)<sub>1</sub> and (3.15) are indeed valid for the periodic loadings as indicated in Fig. 3b. For this reason, the residual stresses may naturally occur on the boundaries  $x = \pm l$ . On the other hand, these series transform the Fourier integrals in the case of  $l \rightarrow \infty$  in  $\lambda = n\pi/l$  and then they can be used for the non-periodic loadings (Girkmann, 1959). By considering  $\Delta\lambda = (\pi/l)\Delta n$ , Eqs. (3.14)<sub>1</sub> and (3.15) can be written respectively, as

$$\sigma_x = \lim_{l \rightarrow \infty} \left[ \frac{2p_0}{\pi} \sum_{\lambda=\pi/l}^{\infty} \frac{\psi(\lambda, y)}{\lambda} \sin(\lambda t) \cos(\lambda x) \Delta\lambda \right] = \frac{2p_0}{\pi} \int_0^{\infty} \frac{\psi(\lambda, y)}{\lambda} \sin(\lambda t) \cos(\lambda x) d\lambda \quad (3.16)$$

$$\sigma_x = \lim_{l \rightarrow \infty} \left[ \frac{P}{\pi} \sum_{\lambda=\pi/l}^{\infty} \psi(\lambda, y) \cos(\lambda x) \Delta\lambda \right] = \frac{P}{\pi} \int_0^{\infty} \psi(\lambda, y) \cos(\lambda x) d\lambda$$

in which, the function  $\psi(\lambda, y)$  in Eqs. (3.16) is the same as  $\psi_n(\lambda, y)$  in Eq. (3.14)<sub>2</sub>.

From the above discussion, the following data would be the inputs in the analysis:  $h = 2d = 1 \text{ mm}$  and  $P = 1 \text{ N}$  in the subsequent analysis. The stress analyses have been performed for the load-distributed width-to-specimen depth ratios  $\beta = 2t/h = t/d = 0, 0.05, 0.1, 0.15, 0.20, 0.25,$  and  $0.29$ . Figure 4 indicates the elastic stress distribution of  $\sigma_x$  at  $x/d = 0, 1, 2$  and  $3$  for  $\beta = 0$  and  $0.25$  obtained from Eqs. (3.16) based on the Fourier integrals (the case of the infinitely long strip). In the analysis, the Gauss-Lagurre method with 100 points has been used for the integration procedure since the analytical solution of Eqs. (3.16) might not be available. It is seen from this figure that  $\sigma_x$  decreases very rapidly with the increasing  $x$  and it becomes approximately zero at  $x/d = 3$  for any  $\beta$  value. A similar result for the elastic stress distribution of  $\sigma_y$  in the middle plane  $y = 0$  was obtained using a different method based on the Fourier integrals by Filon (1903) again for an infinite beam subjected to two equal and opposite concentrated loads (Girkmann, 1959). In addition, Davies and Bose (1968) simulated the splitting beams with the length/depth =  $L/h = 3$  by using the finite element method for  $\beta = 0$  and  $1/12$ .

On the other hand, in the splitting strip specimens, the maximum tensile stress in the plane of loading does not occur at the midpoint ( $x = y = 0$ ), unlike in other splitting specimens. The relative maximum tensile strength values of the splitting strip specimens and other splitting specimens are given for different  $\beta$  values in Fig. 5, comparatively. In this figure, the relative location values ( $y/d$ ) of the maximum tensile stresses are also given for the infinite strip specimens. As shown in Fig. 5, the maximum tensile stress of the strip specimens occurs at the midpoint for  $\beta \geq 0.29$ . Similar to the maximum tensile stress value of the un-notched diagonal splitting-cube specimen, Eq. (3.17) is proposed for the maximum tensile stress value of an un-notched splitting strip specimen in the plane of loading

$$\sigma_{max} = \frac{2P}{\pi b d} \left( \frac{1}{0.7 + 1.685\beta^{0.617}} \right) \quad \beta \leq 0.29 \quad (3.17)$$

The accuracy of Eq. (3.17) is 0.5% for the particular data given in Fig. 5.

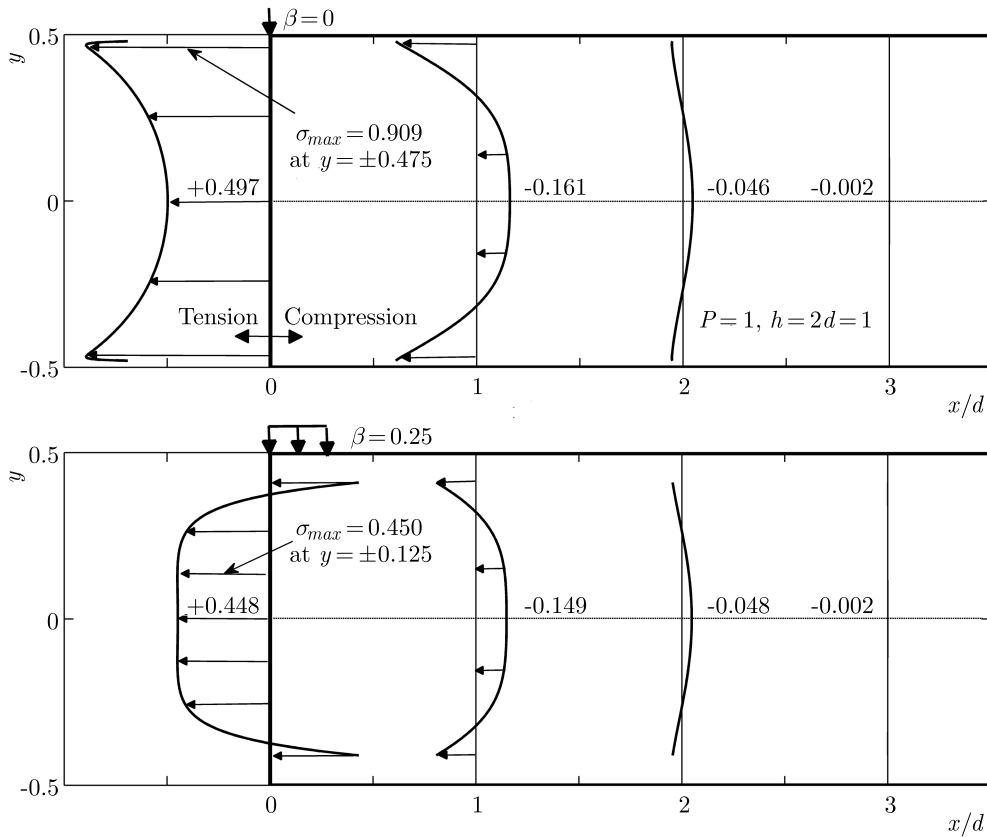


Fig. 4. Stress distribution of  $\sigma_x$  at  $x/d = 0, 1, 2$  and  $3$  for  $\beta = 0$  and  $0.25$  in infinitely long strip

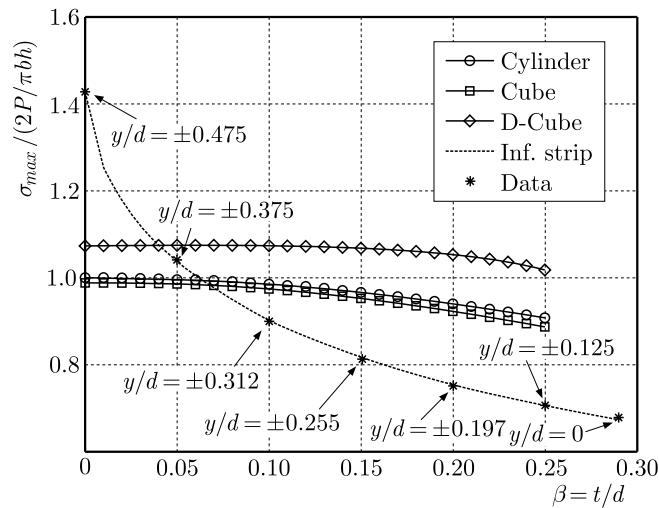


Fig. 5. Comparison of the nominal strengths of split-tension specimens

### 3.2. LEFM formulas

Using the boundary collocation method, Isida (1971) proved that the central cracked plate could be practically regarded as an infinite strip when the length/depth =  $L/h$  ratio of a plate is  $\geq 3$ . Nevertheless, it was indicated in the analysis for Eqs. (3.14)<sub>1</sub> and (3.15) based on the Fourier series for the finite strip with  $L/h = 2$  (Fig. 3b) that the stress distribution of  $\sigma_x$  on the vertical axis at  $x = 0$  was exactly the same as in the case of the infinitely long strip for  $\beta = 0$  to  $0.25$ . This may be explained by Saint-Venant's principle. The sums of the series were continued to be

taken until the absolute value of the  $n$ -th term was less than  $1e-100$ . Consequently, the number of terms ranged from 192 (small  $y$  values) to 340 (large  $y$  values). Meanwhile, similar results were found for certain  $\beta$  values (0.05, 0.10 and 0.20) by Schlee (1978) who studied on a plate with  $L/h = 2$  using the Fourier series. Additionally, in this study, it has also been observed that for  $\sigma_x$  stress distribution along the plane  $x = 0$ , the maximum difference between the solution with  $L/h = 2$  and that of  $L/h = 1.5$  was 0.1%. Nevertheless, it will be seen in the following Sections of this work that this difference is much more significant for a cracked body.

In this study, the analysis of the split-tension strip specimens based on fracture mechanics has been performed for all cases including combinations obtained with  $\alpha$  values of 0.1, 0.2, 0.3, 0.4, 0.5, 0.6, 0.7 and 0.8 and load-distributed width-to-specimen depth ratio values of  $\beta = 0, 0.05, 0.1, 0.15, 0.2, \text{ and } 0.25$ . A parallel analysis was also performed using the boundary element program (BEM). In all analyses, the stress intensity factor  $K_I$  was computed using Eq. (3.1). In practice, the polynomial approach was commonly utilized to interpret normal stresses along the crack line  $\sigma(y)$  in Eq. (3.1) (Anderson 2005). Therefore, in this study, the function of  $\sigma(y)$  was computed at specific points including 0, 0.05, 0.1, 0.15, 0.2, 0.25, 0.3, 0.35 and 0.4 mm on the infinitely long strip with  $h = 2d = 1$  mm and then expressed as the 8th degree polynomial by using the least squares method for each  $\beta$  value. Green's function in Eq. (3.2) was used as the weight function  $m(y, a)$  in Eq. (3.1), since it was essentially equivalent to the weight function, as discussed above. The integration procedures were achieved by means of the Gauss-Chebyshev method.

In this study, the stress intensity factor is defined as follows for the splitting strip specimens

$$K_I = \sigma_N \sqrt{\pi a} Y(\beta, \alpha) \quad (3.18)$$

where  $\sigma_N$  is the nominal stress according to Eq. (2.1),  $a$  is half length of the notch, and  $Y(\beta, \alpha)$  is the geometry factor, where  $\beta$  is the relative load-distributed width ( $t/d$ ) and  $\alpha$  is the relative crack length ( $a/d$ ). The  $Y(\beta, \alpha)$  geometry factors of the splitting specimens are obtained as  $Y(\beta, \alpha) = K_I / (\sigma_N \sqrt{\pi a})$ , where  $K_I$  is calculated from Eq. (3.1).

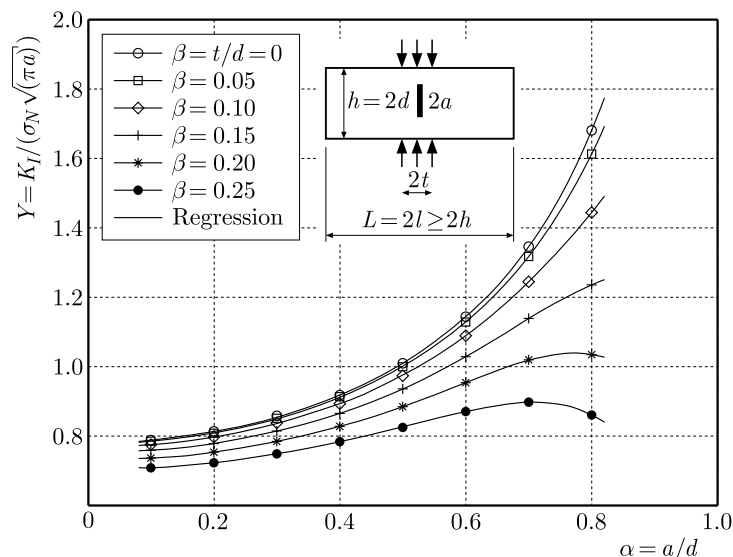


Fig. 6. Geometry factor  $Y(\beta, \alpha)$  values for split-strip specimens

Figure 6 shows the individual geometry factors obtained from the analytical solution; these factors are presented as symbols for each  $\alpha$  and  $\beta$  value. The geometry factors have been generated with the least square method for each  $\beta$  value, as indicated by the curved solid line in Fig. 6. The general form of the selected function is

$$Y(\beta, \alpha) = A_0(\beta) + A_1(\beta)\alpha + A_2(\beta)\alpha^2 + A_3(\beta)\alpha^3 + A_4(\beta)\alpha^4 + A_5(\beta)\alpha^5 \quad (3.19)$$

where the coefficients  $A_i$  ( $i = 0$  to  $5$ ) are functions of  $\beta$ , as summarized in Table 1. Equation (3.19) fits all the results from the analytical solutions with an accuracy of 0.1% for  $0.1 \leq \alpha \leq 0.8$  and any  $\beta$  value. It is emphasized that this accuracy is valid for the strips with  $L/h \geq 2$ , as discussed above.

**Table 1.**  $A_i$  and  $B_i$  coefficients for split-strip specimen

Coefficient	$\beta = t/d$					
	0	0.05	0.10	0.15	0.20	0.25
$A_0$	0.7570	0.7656	0.7781	0.7751	0.7534	0.7200
$A_1$	0.5009	0.2618	-0.1872	-0.4591	-0.4724	-0.3435
$A_2$	-2.8063	-1.1558	1.9581	3.8574	3.9428	2.9948
$A_3$	11.4780	6.2913	-3.6245	-9.9595	-10.7060	-8.1581
$A_4$	-16.6660	-9.2409	5.1032	14.5480	16.0060	12.5460
$A_5$	9.9819	5.9303	-2.0490	-7.6288	-8.9671	-7.5169
$B_0$	0.8882	0.8883	0.8851	0.8733	0.8515	0.82158
$B_1$	1.5494	1.4740	1.3054	1.1399	1.0223	0.94892
$B_2$	-6.0402	-5.5487	-4.4507	-3.3906	-2.6901	-2.3399
$B_3$	16.806	15.2700	11.8060	8.4028	6.0978	4.9091
$B_4$	-21.027	-18.8330	-13.8580	-8.9269	-5.5668	-3.8579
$B_5$	11.503	10.2930	7.5156	4.6857	2.6659	1.5512

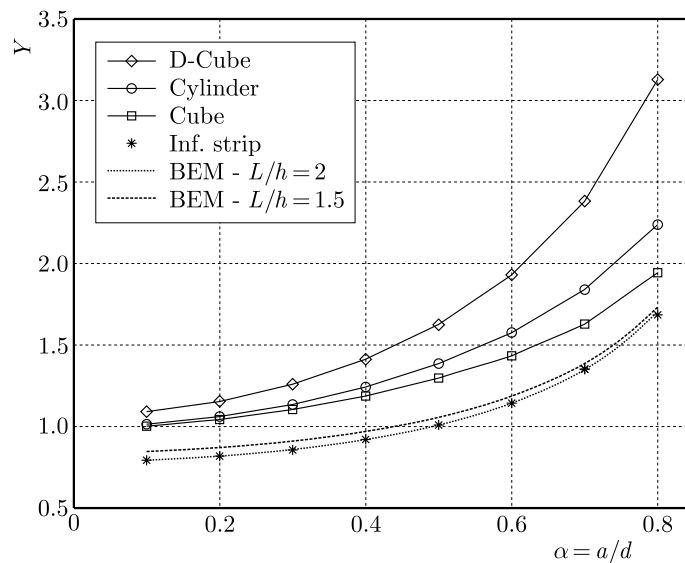


Fig. 7. Comparison of geometry factor  $Y$  values of split-tension specimens for  $\beta = 0$

The variation of the geometry factors is summarized for the splitting specimens, namely: cylinder, cube, diagonal cube and infinite strip for the case of concentrated loading in Fig. 7. The  $Y$  functions of cylindrical and cubical specimens have been obtained from the BEM solutions found in the literature. The BEM solutions for splitting strip specimens with  $L/h = 1.5$  and  $2$  are also given in Fig. 7. A one-quarter model has been used for the plain strain conditions, because of its symmetry in the BEM study. Similar to earlier studies of the author, 250 boundary elements, including 2 crack tip elements, provided reliable results for the crack tip singularity in a one-quarter specimen. The following factors have been the inputs in the analysis: Young's modulus  $E = 1$  MPa, Poisson's ratio  $\nu = 0.2$ ,  $h = 2d = 200$  mm, and  $P = 100$  N. A detailed explanation of the BEM simulations may be seen elsewhere (Ince, 2012a,b). The accuracies of BEM solutions

of the strip specimens are greater than 1.2% for  $L/h = 2$  and better than 7.5% for  $L/h = 1.5$  in comparison with the solution of the infinitely long strip in Fig. 7. On the other hand, the behavior of splitting strips is very different from other splitting specimens, as is clearly shown in Fig. 7. For  $\alpha = 0$ , the value of  $Y$  of strip specimens approach approximately to 0.75, while that of the other specimens approach to 1. Furthermore, the  $Y$  function of the strip is approximately parallel to that of the cube.

Tada *et al.* (2000) proposed that Castigliano's theorem may be used for calculating opening displacements of the crack surface in a cracked body, as follows

$$COD(y) = \frac{2}{E'} \int_{a_F}^a K_{IP} \frac{\partial K_{IF}}{\partial F} da \quad (3.20)$$

where  $K_{IP}$  is the stress intensity factor due to loading forces,  $K_{IF}$  is the stress intensity factor due to virtual forces and  $E' = E/(1 - \nu^2)$  for plane strain and  $E' = E$  for plane stress. In Eq. (3.20),  $a$  is length of the notch and  $a_F$  is location of the virtual force in the vertical distance from the center of the specimen, in which the  $COD$  value is computed (Fig. 2). In this study, Equations (3.18) and (3.1) are used for  $K_{IP}$  and  $K_{IF}$ , respectively. From Eq. (3.20),  $CMOD$  values are computed as follows

$$CMOD = COD(y = 0) = \frac{2}{E'} \int_0^a K_{IP} \frac{\partial K_{IF}}{\partial F} da \quad (3.21)$$

The  $CMOD$  includes not only the elastic constants but also the size of the specimens. The general forms of the specimens are usually described in a polar coordinate system (Tang 1994). Therefore, the  $CMOD$  is defined as follows in this study

$$CMOD = \frac{\pi \sigma_N a}{E'} V_1(\beta, \alpha) \quad (3.22)$$

$V_1(\beta, \alpha)$  dimensionless function in Eq. (3.22) is calculated by normalizing  $CMOD$  values obtained from Eq. (3.21) with  $\pi \sigma_N a / E'$  values. Figure 8 indicates individual  $V_1$  values for each  $\alpha$  and  $\beta$ .

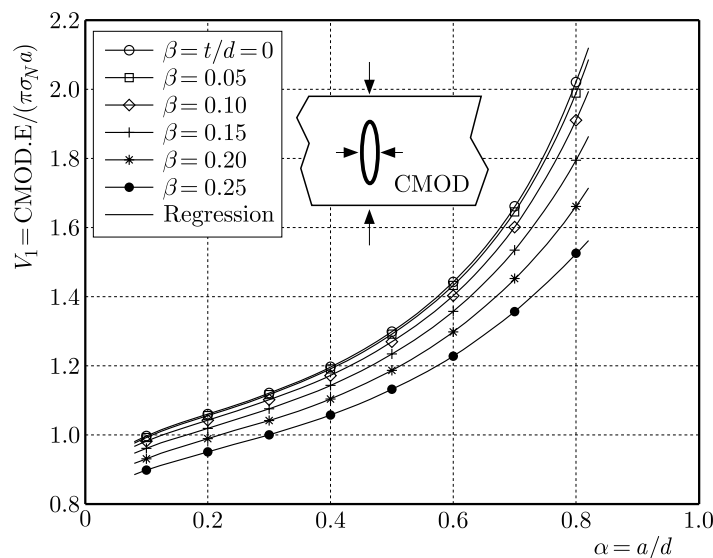


Fig. 8. Non-dimensional  $V_1(\beta, \alpha)$  values for split-strip specimens

The  $V_1(\beta, \alpha)$  values are generated by the least squares method for each  $\beta$ , as depicted in Fig. 8. Similar to Eq. (3.19), the following equation is chosen for the general form of the  $V_1(\beta, \alpha)$  function

$$V_1(\beta, \alpha) = B_0(\beta) + B_1(\beta)\alpha + B_2(\beta)\alpha^2 + B_3(\beta)\alpha^3 + B_4(\beta)\alpha^4 + B_5(\beta)\alpha^5 \quad (3.23)$$

where the coefficients  $B_i$  ( $i = 0, 1, \dots, 5$ ) are functions of  $\beta$  that are listed in Table 1. Equation (3.23) fits all the results from the analytical solutions with an accuracy of 0.2% for  $0.1 \leq \alpha \leq 0.8$  and any  $\beta$  value.

In practice, *COD* values in a cracked body normalize the *CMOD* value to determine the profile of the crack surface. Consequently, the *COD/CMOD* ratio is independent of the specimen size, but does depend on the specimen geometry and loading type (Tang 1994). In this study, the normalized crack profile of the strip specimen is described by means of regression analysis via a formula similar to the earlier form for the cylindrical and cubical specimens proposed by Ince (2012b) as follows

$$\frac{COD(\beta, y, a)}{CMOD} = \sqrt{\left(1 - \frac{y}{a}\right)^2 + \left[2.367 - 0.038(1 + \beta)^{15.9}\alpha^{1.17}\left(\frac{y}{a}\right)^{0.961}\right]\left[\frac{y}{a} - \left(\frac{y}{a}\right)^2\right]} \quad (3.24)$$

in which  $y$  is the vertical distance from the center of the specimen as shown in Fig. 2. The accuracy of the equation is greater than 3.3% for  $0.1 \leq \alpha \leq 0.8$  and any  $\beta$  value.

Equations (3.18) to (3.24) are based on LEFM for split-tension strip specimens. The concrete fracture parameters for effective crack models (two-parameter model, size effect model and double-K model) could easily be calculated using these equations. The coefficients  $A_i$  and  $B_i$  for  $\beta$  values, which are not given in Table 1, could be derived by interpolation.

#### 4. Summary and conclusion

Recently, split-tension specimens such as cylinders, cubes and diagonal cubes have been commonly used to determine the tensile strength of cement-based materials. The split-tension strips have been used to determine the fracture parameters of concrete using the effective crack models such as the two-parameter model, the size effect model and the double-K in this article. Based on these theoretical and numerical investigations, the following conclusions can be drawn:

- The number of theoretical and experimental studies on split-tension strip specimens is limited. Therefore, in this study, a formula for the maximum tensile strength of concrete has been developed for un-notched strip specimens. The results of the analysis reveal that the derived formula is valid for strips with the ratio of length/depth =  $L/h \geq 2$  both for the Fourier integral (the case of the infinite long strip) and the Fourier series (the case of the finite strip). Similarly, it has been indicated from the parallel analysis, which was based on the boundary element method, that the LEFM formulas of cracked strip specimens are valid for strips with  $L/h \geq 2$ .
- The initial crack of the splitting strip specimens starts at about the location of the loading point, while the initial crack in other splitting specimens starts at the center of the section. However, the initial crack location approximates to the center of the section with the increasing load-distributed width-to-specimen depth ratios  $\beta$ , and it is in the center of the section for  $\beta \geq 0.29$ .
- In this study, only double symmetrical strips have been analyzed and they have no vertical displacement and no shear stress at the middle line  $y = 0$ , as is clearly shown in Fig. 3. Consequently, by considering the upper half of the strip ( $L/d \geq 4$ ), the results of this study may also be utilized in the analysis of a cracked elastic layer resting on a rigid smooth base in soil and rock mechanics. This problem was investigated by Marguerre (1931) for uncracked elastic layers.

## References

1. ANDERSON T.L., 2005, *Fracture Mechanics: Fundamentals and Applications*, CRC Press, Boca Raton
2. BARBER J.R., 2002, *Elasticity*, Kluwer Academic Publishers, Dordrecht
3. BASU S., MANDAL S.C., 2016, P-wave interaction with a pair of rigid strips embedded in an orthotropic strip, *Journal of Theoretical and Applied Mechanics*, **54**, 2, 579-592
4. BAZANT Z.P., KAZEMI M.T., 1990, Determination of fracture energy, process zone length, and brittleness number from size effect with application to rock and concrete, *International Journal of Fracture*, **44**, 2, 111-131
5. BUECKNER H.F., 1970, A novel principle for the computation of stress intensity factors, *Zeitschrift für Angewandte Mathematik and Mechanik*, **50**, 9, 529-546
6. CARNEIRO F.L., BARCELLOS A., 1949, Tensile strength of concrete (in French), *RILEM Bulletin*, **13**, 98-125
7. DAVIES J.D., BOSE D.K., 1968, Stress distribution in splitting tests, *ACI Journal*, **65**, 662-669
8. FILON L.N.G., 1903, On the approximate solution of the bending of a beam of rectangular section, *Transaction of the Royal Society of London Series (A)*, **201**, 63-155
9. GDOUTOS E.E., 1990, *Fracture Mechanics Criteria and Applications*, Kluwer Academic Publishers, London
10. GIRKMANN K., 1959, *Plate and Shell Structures* (in German), Springer-Verlag Wien
11. INCE R., 2010, Determination of concrete fracture parameters based on two-parameter and size effect models using split-tension cubes, *Engineering Fracture Mechanics*, **77**, 2233-2250
12. INCE R., 2012a, Determination of concrete fracture parameters based on peak-load method with diagonal split-tension cubes, *Engineering Fracture Mechanics*, **82**, 100-114
13. INCE R., 2012b, Determination of the fracture parameters of the double-K model using weight functions of split-tension specimens, *Engineering Fracture Mechanics*, **96**, 416-432
14. INCE R., GÖR M., EREN M.E., ALYAMAÇ K.E., 2016, The effect of size on the splitting strength of cubic concrete members, *Strain*, **51**, 2, 135-146
15. INCE R., GÖR M., ALYAMAÇ K.E., EREN M.E., 2016, Multi-fractal scaling law for split strength of concrete cubes, *Magazine of Concrete Research*, **68**, 3, 141-150
16. ISIDA M., 1971, Effect of width and length on stress intensity factors of internally cracked plates under various boundary conditions, *International Journal of Fracture*, **7**, 3, 301-316
17. JENQ Y.S., SHAH S.P., 1985, Two-parameter fracture model for concrete, *Journal of Engineering Mechanics, ASCE*, **111**, 10, 1227-1241
18. MARGUERRE K., 1931, Pressure distribution by an elastic layer on a rigid rough layer (in German), *Ingenieur-Archiv*, **2**, 108-117
19. MIRSAIMOV V.M., HASANOV S.G., 2015, Effect of damages on crack development in coating on elastic foundation, *Journal of Theoretical and Applied Mechanics*, **53**, 4, 823-836
20. MODEER M., 1979, A fracture mechanics approach to failure analyses of concrete materials, Report TVBM-1001, Division of Building Materials, University of Lund, Sweden
21. NALLATHAMBI P., KARIHALOO B.L., 1986, Determination of the specimen size independent fracture toughness of plain concrete, *Magazine of Concrete Research*, **38**, 135, 67-76
22. NEVILLE A.M., 2011, *Properties of Concrete*, Pearson Education Limited, Essex, UK.
23. NILSSON S., 1961, The tensile strength of concrete determined by splitting tests on cubes, *RILEM Bulletin*, **11**, 63-67

24. RICE J.R., 1972, Some remarks on elastic crack-tip stress fields, *International Journal of Solid Structures*, **8**, 751-758
25. ROCCO C., GUINEA G.V., PLANAS J., ELICES M., 1995, The effect of the boundary conditions on the cylinder splitting strength, *Proceedings of FRAMCOS-2: Aedificatio Publishers*, 75-84, Freiburg, Germany
26. SCHLEE W.S., 1978, Determination of the tensile strength of concrete (in German), *Beton*, **28**, 2, 57-62
27. TADA H., PARIS P.C., IRWIN G.R., 2000, *Stress Analysis of Cracks Handbook*, ASME Press, New York
28. TANG T., 1994, Effect of load-distributed width on split tension of unnotched and notched cylindrical specimens, *Journal of Testing and Evaluation*, *ASTM*, **22**, 401-409
29. TANG T., OUYANG C., SHAH S.P., 1996, A simple method for determining material fracture parameters from peak loads, *ACI Materials Journal*, **93**, 2, 147-157
30. TANG T., SHAH S.P., OUYANG C., 1992, Fracture mechanics and size effect of concrete in tension, *Journal of Structural Engineering*, *ASCE*, **118**, 3169-3185
31. TIMOSHENKO S.P., GODIER J.N., 1970, *Theory of Elasticity*, Mc-Graw Hill, New York, USA
32. TWEED J., DAS S.C., ROOKE D.P., 1972, The stress intensity factor of a radial crack in a finite elastic disc, *International Journal of Engineering Science*, **10**, 323-335
33. XU S., REINHARDT H.W., 1999, Determination of double-K criterion for crack propagation in quasi-brittle fracture, Part I: Experimental investigation of crack propagation, *International Journal of Fracture*, **98**, 2, 111-149

*Manuscript received November 9, 2016; accepted for print December 12, 2016*